Applied Acoustics 73 (2012) 323–337

Contents lists available at SciVerse ScienceDirect

Applied Acoustics

journal homepage: www.elsevier.com/locate/apacoust

Acoustic transmission performance of double-wall active sound packages in a tube: Numerical/experimental validations

Y. Hu [a,*], M.A. Galland [b], Kean Chen [c]

[a] Structures Department, Shanghai Aircraft Design and Research Institute, Shanghai 200232, PR China
[b] Centre Acoustique, LMFA, Ecole Centrale de Lyon, Ecully 69134, France
[c] College of Marine Engineering, Northwestern Polytechnical University, Xi'an 710072, PR China

ARTICLE INFO

Article history:
Received 20 April 2010
Received in revised form 9 October 2011
Accepted 11 October 2011
Available online 5 November 2011

Keywords:
Active noise control
Double-wall sound package
Transmission loss
Porous material

ABSTRACT

A method based on the combination of the (u,p) formulation and the finite element approach is proposed for calculating the transmission loss of double-wall active sound packages with porous-material cores in a rectangular tube. The (u,p) formulation based on the displacement in the solid phase and the pressure in the fluid phase is rewritten to investigate sound propagation in porous materials, and the coupled boundary conditions and related parameters involved are given. The transmission loss of the double-wall active sound packages excited by a plane wave is calculated via the COMSOL environment with passive and active control. Moreover, a two source-location method is developed to measure the transmission loss of these double-wall active sound packages in a rectangular tube. Some results from numerical examples are shown to be in good agreement with the measured data. It is concluded that with active control, the transmission loss of double-wall active sound packages can be improved by more than 10 dB around resonance frequencies.

1. Introduction

Finite multilayer systems are widely used for noise control in automobiles, aircrafts, buildings and other engineering applications. A particular example of such multilayer systems is a double-wall structure, which is composed of two elastic plates (called an 'excited plate' and a 'radiating plate,' respectively) and a core, such as an air gap or highly dissipative medium. Indeed, porous material has been commonly used as a passive core for reducing both structural and airborne sound in double-wall systems because of its ability to dissipate acoustical energy in the medium. Nevertheless, it is well known that such double-wall passive packages with porous-material cores are efficient enough at medium and high frequencies but exhibit poor performance at low frequencies, where the resonance inherent to the layer distribution occurs. As an alternative to passive control, active control appears to be a possible approach for remedying this problem. Since active control was proposed by Leug [1], many researchers have proceeded to use it to reduce structural vibration and acoustic transmission at low frequencies and some progress has been achieved [2–15]. Guigou and Fuller [5] and Johnson and Fuller [6] introduced a smart skin for reducing the noise transmitted into an aircraft, using an efficient piezoelectric actuator as a secondary source. Pan and Bao [7] presented a theoretical model for active control of sound transmission through double-panels, in which three different control arrangements were investigated. Using control loudspeakers inside the air gap, Fonseca et al. [8] experimentally demonstrated that active sound transmission reduction could be achieved by reducing the energy transmission through the gap. After a few years, Carneal and Fuller [10] developed a robust analytical model of a simply supported plate-air-plate system, finding an optimal position for piezoelectric patches. Lee and his colleagues [13] demonstrated some experimental results obtained with a hybrid concept involving a double-plate panel with a porous-material core and active control. Over the past decade, the LMFA, Centre Acoustique, at École Centrale de Lyon has developed a design for a hybrid broadband absorbing liner that combines the passive properties of absorbent materials with active control [15]. The sound transmission performance of these double-wall active sound packages is of utmost importance for noise control, and the demand for tools to predict their acoustical and structural behavior has increased considerably.

Due to the biphasic nature of a porous material, the characterization of its acoustical behaviour is crucial to predict the acoustical performance of double-wall systems with porous-material cores. For high-frequency excitation or porous materials attached to a rigid wall structure, the porous material is often considered as an equivalent fluid with an effective density and bulk modulus [16]. This type of modeling applies to porous materials having either a rigid skeleton (i.e., motionless) or a very limp skeleton

* Corresponding author. Tel.: +86 13701998591.
E-mail address: huying_nwpu@hotmail.com (Y. Hu).

0003-682X/$ - see front matter © 2011 Elsevier Ltd. All rights reserved.
doi:10.1016/j.apacoust.2011.10.003

[17–19]. In this case, only one compression wave propagates in the air-saturated medium, and five important parameters are needed to define the equivalent density and the equivalent impedance: porosity, resistivity, tortuosity, viscous length and thermal length [20]. Hence, Helmholtz's equation is a governing equation in the porous material.

For low-frequency excitation or porous materials attached to an elastic plate, the porous material bears three basic waves propagating simultaneously in the solid and fluid phases: two compression waves and one shearing wave. In this case, the elasticity of the skeleton should be considered, and the strong coupling between the solid and fluid phases cannot be ignored. The mechanical behavior of poroelastic materials has been established by Biot's theory describing the propagation of elastic waves [21]. For several decades, many efforts were made to adapt Biot's theory to specific acoustic problems in porous materials using the finite element method [22–28]. Following these works, the equations of dynamic equilibrium of the porous medium were solved in terms of the solid and fluid displacements: u describing the displacement of the solid phase, and U describing the displacement of the fluid phase. The first model [25,26], motivated by biomedical and geomechanical problems, was based on classical plate theory with Kirchhoff's assumptions and the (u,U) formulation of Biot's relations. More recently, Leclaire et al. [27] used the (u,U) formulation of Biot's equations to derive two equations of equilibrium for the porous plate. The main advantages of this model are the simplicity of the equations and the fact that they can be solved under boundary conditions other than simply supported edges. This model has been validated by experiments on high-density clamped porous plates [28]. For simple one-or two-dimensional structures, the vibro-acoustic responses can be accurately calculated by the finite element method with the (u,U) formulation; however, for complex three-dimensional structures, at least six degrees of freedom per node are required to calculate the vibration response, which leads to cumbersome calculations for large finite element models and spectral analysis.

To alleviate these difficulties, a mixed formulation using the displacement of the solid phase and the interstitial fluid pressure as variables was proposed by Atalla et al. [29]. This formulation, called the (u,p) formulation, seems more suitable for large finite element models and requires only four degrees of freedom per node. Lately, the strain couplings between the fluid and solid phases of porous materials have been derived according to the continuity of the solid-phase displacement vector and the interstitial fluid pressure [30]. However, because of the biphasic nature of porous materials, in the case of broadband source excitation, excessive computing difficulties persist in finite element models; hence, the (u,p) formulation must be simplified according to the characteristics of the solid and fluid media. Dazel et al. [31–34] proposed a simplified (u,p) formulation based on the dominant vibration modes of porous materials; Bermudez [35] presented a simplified finite element model for porous materials with a non-viscous and pore-interlinked fluid medium; and Batifol [36] deduced the partial differential equations of porous materials in the COMSOL environment based on the (u,p) formulation. Etchessahar et al. used the (u,p) formulation of Biot's equations in association with the classical theory of plates to derive two coupled equations of equilibrium of a homogeneous and isotropic poroelastic plate [37,38]. This theory is valid in the case of porous materials as long as the wavelength of the bending waves is much greater than the size of the pores. Because of these simplified finite element models, the (u,p) formulation has been widely used to model sound propagation in porous materials.

Another effective approach to predicting transmission loss is direct measurement. Generally speaking, the reverberation room method [39] and the standing wave tube method [40] are the two most useful methods that have been widely applied to measure the acoustical properties of a certain material. In fact, the reverberation room method provides authoritative test results, but it is difficult to apply. This method not only takes time but also requires some specialized equipment, such as a reverberation room and a high-quality microphone. In addition, this method requires the dimensions of the tested structure to be somewhat large.

To remedy the drawbacks of the reverberation room method, the standing wave tube method, which can measure the acoustic properties of small-dimensioned structures, has also been used widely and adopted as an ISO standard [40]. Apfel et al. [41] developed a new laboratory method to evaluate the acoustical properties of expandable sealants and other automotive sealants in the standing wave tube. Song and Bolton [42] described a two-microphone standing wave tube method for evaluating the acoustical properties of homogeneous and isotropic porous materials based on the transfer matrix method. Zhu et al. [43–45] proposed a four-microphone method to measure sound transmission loss in the standing wave tube. This method can separate the transmission wave from the reflected wave in the absorbent end and improve the precision of the measurement in the low-frequency range.

Nevertheless, the major drawback of the standing wave tube method is that an anechoic termination is required. In principle, an anechoic termination could be constructed using a long exhaust tube, highly absorbent materials, horn-shaped pipes or an active anechoic termination [46]. However, a fully anechoic termination is difficult to build, particularly one that is effective at low frequencies. Thus, two alternative measurement approaches, which do not require an anechoic termination, are considered: the two-load method [47] and the two source-location method [48]. Both methods are realized by measuring acoustic pressures at four fixed locations, two upstream and two downstream of the tested structure, with a different load (two-load method) or a random source (two-source-location method) on both sides of the test tube. Then the four-pole parameters of the tested structure are calculated by means of a dual-channel FFT analyzer and time-domain ensemble averaging. The two-load method suffers from an additional disadvantage in that the two loads may not be sufficiently different at all frequencies of interest, so the two source-location method is much more stable and entirely independent of the loading terminations.

This study aims to develop a finite element model of double-wall active sound packages with the (u,p) formulation in the COMSOL environment based on Batifol's accomplishments [36]. The partial differential equation of the porous material is described with the COMSOL formulation, and the couplings between the porous material and the air gap, between the porous material and the elastic plate, and between two different porous materials are formulated in COMSOL environment. The model is validated by describing the normal surface impedance for the analytically solved case of a one-dimensional porous material with three boundary conditions: bonded to a rigid wall, attached with a layer of air, and under an active control condition with zero pressure in the rear of the porous medium. Secondly, the dynamic responses of some double-wall active sound packages, in which piezoelectric patches are added onto the excited plate to serve as secondary vibrational sources and enhance the sound packages' effectiveness at low and/or resonance frequencies, are studied. The properties of different layers in these double-wall active sound packages are tested and compared to the numerical results in the COMSOL environment. Lastly, the sound transmission performance of the double-wall active sound packages is described in terms of transmission loss (TL_{dB}) and validated by experimental data obtained in the tube with the two-source-location method [48], using a dSPACE-DS1103 controller implemented with Simulink to find the optimal value of the secondary sound source.

2. Theories

2.1. The (u,p) formulation for poroelastic medium

The motion of poroelastic media can be described by the macroscopic displacement of the solid phase and the sound pressure of the fluid phase represented respectively by u and p. This classical displacement–pressure (u,p) formulation, proposed by Atalla et al. [29] based on Biot's poroelasticity equation, can be written in the form of

$$\nabla \cdot \hat{\boldsymbol{\sigma}}^{\mathbf{s}}(\mathbf{u}^{\mathbf{s}}) + \omega^2 \tilde{\rho}\mathbf{u}^{\mathbf{s}} + \tilde{\gamma}\nabla p = 0, \tag{1-a}$$

$$\nabla^2 p + \omega^2 \tilde{\rho}_{22} p/R - \omega^2(\tilde{\rho}_{22}\tilde{\gamma}/\phi^2)\nabla \cdot \mathbf{u}^{\mathbf{s}} = 0, \tag{1-b}$$

where the tilde symbol indicates that the associated physical property is complex and frequency dependent. In Eq. (1), ω is the angular frequency, $\mathbf{u}^{\mathbf{s}}$ and p respectively denote the solid macroscopic displacement vector and the fluid sound pressure. $\hat{\boldsymbol{\sigma}}^{\mathbf{s}}$ denotes the modified partial stress tensor associated with the skeleton particle and only depends on the displacement of the solid phase. ϕ stands for the porosity defined as the ratio between the volume of the fluid phase and the total volume of the porous material, $\tilde{\rho}_{22}$ is the modified Biot's density of the fluid phase accounting for viscous dissipation. $\tilde{\rho}$ is an effective density given by $\tilde{\rho} = \tilde{\rho}_{11} - (\tilde{\rho}_{12})^2/\tilde{\rho}_{22}$ where $\tilde{\rho}_{11}$ is the modified Biot's density of the solid phase accounting for viscous dissipation. $\tilde{\rho}_{12}$ is the modified Biot's density which accounts for the interaction between the inertia forces of the solid and fluid phases together with viscous dissipation. The coefficient $\tilde{\gamma}$ is given by $\tilde{\gamma} = \phi(\tilde{\rho}_{12}/\tilde{\rho}_{22} - Q/R)$ where Q is an elastic coupling coefficient between the two phases; R is interpreted as the bulk modulus of the air occupying a fraction of the unit volume aggregate.

In consequence, Eq. (1-a) is the solid phase equation in terms of the (u,p) formulation, and the first two terms represent the elastodynamic equation of the material in vacuo. Eq. (1-b) is exactly the classical equivalent fluid equation for absorbing media, and the first two terms represent the dynamic behavior of the material when its frame is supposed motionless. The third term in both equations couple the dynamic of the two phases.

2.2. The finite element model for poroelastic medium

The acoustic wave propagation in the double-wall active sound package is calculated by the finite element method and corresponding models can be founded in Comsol environment. Comsol provides powerful application modes for acoustic, piezoelectric and elastic problems, but it does not currently provide a specific application mode for the poroelastic medium. Since the coupling between the fluid and solid phases occurs in the poroelastic medium, the partial differential equation (PDE mode) provided by Comsol is chosen for modeling the poroelastic material [36]. The partial differential equation can be rewritten here as follows:

$$\begin{aligned} &\boldsymbol{\Gamma} \cdot \nabla = \mathbf{F} \\ &-\boldsymbol{\Gamma} \cdot \mathbf{n} = \mathbf{G} + (\partial \mathbf{L}/\partial \mathbf{U})^T l \\ &0 = \mathbf{L}, \end{aligned} \tag{2}$$

Here, $\mathbf{U}$ is the vector of unknowns and $\boldsymbol{\Gamma}$, $\mathbf{F}$, $\mathbf{G}$, $\mathbf{L}$ are PDE coefficients depending on $\mathbf{U}$ or its differentiation, $\mathbf{L}$ and $\mathbf{G}$ represent the 'Dirichlet' and 'Neumann' vector respectively, l denotes the Lagrange multiplier; $\mathbf{n}$ is the outward normal unit vector. The first term in Eq. (2) is the partial differential equation of variable $\mathbf{U}$, and the last two terms denote respectively the Dirichlet and Neumann boundary condition of porous materials.

In Cartesian coordinate system, the displacement of the solid phase is presented by $\mathbf{u}^{\mathbf{s}} = (u, v, w)$, whereas the pressure of the fluid phase is described by p. Comparing the first term of Eq. (2) to Eq. (1), $\boldsymbol{\Gamma}$ and $\mathbf{F}$ can be written as follows:

$$\boldsymbol{\Gamma} = \begin{bmatrix} \Gamma_{ij} \\ \Gamma_{4j} \end{bmatrix} = \begin{bmatrix} \hat{\boldsymbol{\sigma}}^{\mathbf{s}}(\mathbf{u}^{\mathbf{s}}) \\ \nabla p \end{bmatrix}, \tag{3}$$

$$\mathbf{F} = \begin{bmatrix} F_i \\ F_4 \end{bmatrix} = \begin{bmatrix} -\omega^2 \tilde{\rho}\mathbf{u}^{\mathbf{s}} - \tilde{\gamma}\nabla p \\ -\omega^2 \tilde{\rho}_{22} p/R + \omega^2(\tilde{\rho}_{22}\tilde{\gamma}/\phi^2)\nabla \cdot \mathbf{u}^{\mathbf{s}} \end{bmatrix}, \tag{4}$$

According to the definition in Ref. [29], the expression of $\hat{\boldsymbol{\sigma}}^{\mathbf{s}}(\mathbf{u}^{\mathbf{s}})$ can be written as

$$\hat{\boldsymbol{\sigma}}^{\mathbf{s}}(\mathbf{u}^{\mathbf{s}}) = (A - Q^2/R)\nabla \cdot \mathbf{u}^{\mathbf{s}} + 2N\boldsymbol{\varepsilon}^{\mathbf{s}}, \tag{5}$$

where A is the Lamé coefficient for the elastic solid.

Defining $u^s_{k,k} = \nabla \cdot \mathbf{u}^{\mathbf{s}} = \partial u/\partial x + \partial v/\partial y + \partial w/\partial z = u_x + v_y + w_z$, $\boldsymbol{\Gamma}$ and $\mathbf{F}$ can be rewritten in details as

$$\boldsymbol{\Gamma} = \begin{bmatrix} 2Nu_x + \widehat{A}u^s_{k,k} & N(u_y + v_x) & N(u_z + w_x) \\ N(u_y + v_x) & 2Nv_y + \widehat{A}u^s_{k,k} & N(w_y + v_z) \\ N(u_z + w_x) & N(v_z + w_y) & 2Nw_z + \widehat{A}u^s_{k,k} \\ p_x & p_y & p_z \end{bmatrix}, \tag{6}$$

$$\mathbf{F} = \begin{bmatrix} -\omega^2 \tilde{\rho}u - \tilde{\gamma}p_x \\ -\omega^2 \tilde{\rho}v - \tilde{\gamma}p_y \\ -\omega^2 \tilde{\rho}w - \tilde{\gamma}p_z \\ -\omega^2 \tilde{\rho}_{22} p/R + \omega^2 \tilde{\rho}_{22}\tilde{\gamma}u^s_{k,k}/\phi^2 \end{bmatrix}, \tag{7}$$

Here $\widehat{A} = A - Q^2/R$, N is shearing modulus of the poroelastic medium; the subscripts 'x', 'y' and 'z' represent the derivation of x, y, z.

2.3. Coupling boundary conditions

The poroelastic/air, poroelastic/elastic and poroelastic/poroelastic couplings will be presented in this section. Simpler boundary conditions (a rigid wall, imposed pressure, imposed displacements) can be directly derived from these formulations, described below.

2.3.1. Poroelastic/air coupling

In the case of a poroelastic medium linked to an acoustic medium, Eq. (8) describes the continuity conditions of the total normal stress, acoustic pressure and fluid flow [30].

$$\begin{aligned} &\boldsymbol{\sigma}^{\mathbf{t}} \cdot \mathbf{n} = -p^a \cdot \mathbf{n} \\ &p = p^a \\ &(1-\phi)\mathbf{u}^{\mathbf{s}} \cdot \mathbf{n} + \phi \mathbf{U}^{\mathbf{f}} \cdot \mathbf{n} = (\rho_0 \omega^2)^{-1} \nabla p^a \cdot \mathbf{n}. \end{aligned} \tag{8}$$

Here, p^a is the pressure in the acoustic medium, $\boldsymbol{\sigma}^{\mathbf{t}}$ is the total stress tensor in the poroelastic material, $\mathbf{U}^{\mathbf{f}}$ is the displacement of the fluid phase in the (u,U) formulation, and $\mathbf{n}$ is the outward normal unit vector.

The detailed expressions for $\mathbf{U}^{\mathbf{f}}$ and $\boldsymbol{\sigma}^{\mathbf{t}}$ were given by Atalla et al. [29] as follows:

$$\mathbf{U}^{\mathbf{f}} = (\phi/\omega^2 \tilde{\rho}_{22})\nabla p - (\tilde{\rho}_{12}/\tilde{\rho}_{22})\mathbf{u}^{\mathbf{s}}, \tag{9}$$

$$\begin{aligned} \boldsymbol{\sigma}^{\mathbf{t}} &= \boldsymbol{\sigma}^{\mathbf{t}}(\mathbf{u}^{\mathbf{s}}, \mathbf{U}^{\mathbf{f}}) = \boldsymbol{\sigma}^{\mathbf{s}}(\mathbf{u}^{\mathbf{s}}, \mathbf{U}^{\mathbf{f}}) + \boldsymbol{\sigma}^{\mathbf{f}}(\mathbf{u}^{\mathbf{s}}, \mathbf{U}^{\mathbf{f}}) \\ &= \hat{\boldsymbol{\sigma}}^{\mathbf{s}}(\mathbf{u}^{\mathbf{s}}) - \phi(1 + Q/R)p. \end{aligned} \tag{10}$$

Using Eq. (10), the first two equations of Eq. (8) can be transformed into

$$\begin{aligned} &\hat{\boldsymbol{\sigma}}^{\mathbf{s}}(\mathbf{u}^{\mathbf{s}}) \cdot \mathbf{n} = -[1 - \phi(1 + Q/R)]p^a \cdot \mathbf{n} \\ &\nabla p \cdot \mathbf{n} = \nabla p^a \cdot \mathbf{n} = 0 \\ &p - p^a = 0. \end{aligned} \tag{11}$$

Substituting Eq. (9) into the third equation of Eq. (8) gives the correct normal acceleration as written in Eq. (12).

$$\nabla p^a \cdot \mathbf{n}/\rho_0 = \omega^2[\mathbf{u^s}\cdot\mathbf{n}(1-\phi(1+\tilde{\rho}_{12}/\tilde{\rho}_{22}))] + (\phi^2/\tilde{\rho}_{22})\nabla p\cdot\mathbf{n}, \tag{12}$$

Eq. (12) shows that the coupling effect between a porous material and an air gap behaves as acceleration into the air layer.

By comparing Eq. (11) with the last two terms of Eq. (2), the well-formulated vectors **G** and **L** can be expressed as

$$\mathbf{G} = \begin{bmatrix} [1-\phi(1+Q/R)]p^a n_x \\ [1-\phi(1+Q/R)]p^a n_y \\ [1-\phi(1+Q/R)]p^a n_z \\ 0 \end{bmatrix}, \quad \mathbf{L} = \begin{bmatrix} 0 \\ 0 \\ 0 \\ p-p^a \end{bmatrix}. \tag{13}$$

2.3.2. Poroelastic/elastic coupling

Suppose the poroelastic material is bonded onto an elastic solid, enforcing total continuity between the solid phase and elastic displacements. The continuities of the total normal stress, displacement and no fluid flow at the interface are conserved as follows [30]:

$$\begin{aligned} &\boldsymbol{\sigma}^{\mathbf{t}}\cdot\mathbf{n} = \sigma^{\mathbf{e}}\cdot\mathbf{n} \\ &\mathbf{u^s} = \mathbf{u^e} \\ &\mathbf{U^f}\cdot\mathbf{n} - \mathbf{u^s}\cdot\mathbf{n} = \mathbf{0}, \end{aligned} \tag{14}$$

Here, $\boldsymbol{\sigma}^{\mathbf{e}}$ is the total stress tensor in the poroelastic material.

Eq. (14) can be rewritten as follows by substituting (9) and (10):

$$\begin{aligned} &\hat{\boldsymbol{\sigma}}^{\mathbf{s}}(\mathbf{u^s})\cdot\mathbf{n} = \phi(1+Q/R)p\cdot\mathbf{n} + \boldsymbol{\sigma}^{\mathbf{e}}\cdot\mathbf{n} \\ &\nabla p\cdot\mathbf{n} = \omega^2/\phi(\tilde{\rho}_{12}+\tilde{\rho}_{22})\mathbf{u^s}\cdot\mathbf{n} \\ &\mathbf{u^e} - \mathbf{u^s} = 0. \end{aligned} \tag{15}$$

By comparing Eq. (15) to the last two terms of Eq. (2), the well-formulated vectors **G** and **L** can be expressed as

$$\mathbf{G} = \begin{bmatrix} -\phi(1+Q/R)pn_x - \left(\sigma^e_{xx}n_x + \sigma^e_{xy}n_y + \sigma^e_{xz}n_z\right) \\ -\phi(1+Q/R)pn_y - \left(\sigma^e_{xy}n_x + \sigma^e_{yy}n_y + \sigma^e_{yz}n_z\right) \\ -\phi(1+Q/R)pn_z - \left(\sigma^e_{xz}n_x + \sigma^e_{yz}n_y + \sigma^e_{zz}n_z\right) \\ -(\omega^2/\phi)(\tilde{\rho}_{12}+\tilde{\rho}_{22})(un_x + vn_y + wn_z) \end{bmatrix}, \quad \mathbf{L} = \begin{bmatrix} u^e - u^s \\ v^e - v^s \\ w^e - w^s \\ 0 \end{bmatrix}. \tag{16}$$

2.3.3. Poroelastic/poroelastic coupling

In the case of a poroelastic medium linked to another poroelastic medium, the continuity conditions of the total normal stress, the displacements of the solid and fluid phases and the fluid flow can be described by the following equation [30]:

$$\begin{aligned} &\boldsymbol{\sigma}^{\mathbf{t}}_{\mathbf{1}}\cdot\mathbf{n} = \boldsymbol{\sigma}^{\mathbf{t}}_{\mathbf{2}}\cdot\mathbf{n} \\ &\mathbf{u^s_1} = \mathbf{u^s_2} \\ &p^s_1 = p^s_2, \\ &\phi_1\left(\mathbf{U^f_1}\cdot\mathbf{n} - \mathbf{u^s_1}\cdot\mathbf{n}\right) = \phi_2\left(\mathbf{U^f_2}\cdot\mathbf{n} - \mathbf{u^s_2}\cdot\mathbf{n}\right). \end{aligned} \tag{17}$$

Substituting Eqs. (9) and (10) into (17), for the poroelastic medium 1, yields

$$\begin{aligned} &\hat{\boldsymbol{\sigma}}^{\mathbf{s}}_{\mathbf{1}}(\mathbf{u^s_1})\cdot\mathbf{n} = \hat{\boldsymbol{\sigma}}^{\mathbf{s}}_{\mathbf{2}}(\mathbf{u^s_2})\cdot\mathbf{n} + \left[\phi_1\left(1+\frac{Q_1}{R_1}\right) - \phi_2\left(1+\frac{Q_2}{R_2}\right)\right]p_1\cdot\mathbf{n}, \\ &\nabla p_1\cdot\mathbf{n} = \omega^2\frac{\phi_2^2}{\phi_1^2}\nabla p_2\cdot\mathbf{n} + \omega^2\left(\frac{\tilde{\rho}^{(1)}_{12}+\tilde{\rho}^{(1)}_{12}}{\phi_1^2} - \frac{\tilde{\rho}^{(2)}_{12}+\tilde{\rho}^{(2)}_{12}}{\phi_2^2}\right)\mathbf{u^s_1}\cdot\mathbf{n}. \end{aligned} \tag{18}$$

For the poroelastic medium 2:

$$\begin{aligned} &\hat{\boldsymbol{\sigma}}^{\mathbf{s}}_{\mathbf{2}}(\mathbf{u^s_2})\cdot\mathbf{n} = \hat{\boldsymbol{\sigma}}^{\mathbf{s}}_{\mathbf{1}}(\mathbf{u^s_1})\cdot\mathbf{n} + \left[\phi_2\left(1+\frac{Q_2}{R_2}\right) - \phi_1\left(1+\frac{Q_1}{R_1}\right)\right]p_2\cdot\mathbf{n} \\ &\nabla p_2\cdot\mathbf{n} = \omega^2\frac{\phi_1^2}{\phi_2^2}\nabla p_1\cdot\mathbf{n} + \omega^2\left(\frac{\tilde{\rho}^{(2)}_{12}+\tilde{\rho}^{(2)}_{12}}{\phi_2^2} - \frac{\tilde{\rho}^{(1)}_{12}+\tilde{\rho}^{(1)}_{12}}{\phi_1^2}\right)\mathbf{u^s_2}\cdot\mathbf{n}. \end{aligned} \tag{19}$$

By comparing Eqs. (18) and (19) to the last two terms of Eq. (2), the well-formulated vectors **G** and **L** can be expressed as

$$\mathbf{G_1} = -\mathbf{A_1\Gamma_2}\cdot\mathbf{n} - \mathbf{B_1}, \tag{20}$$

$$\mathbf{G_2} = -\mathbf{A_2\Gamma_1}\cdot\mathbf{n} - \mathbf{B_2}, \tag{21}$$

$$\mathbf{L_1} = -\mathbf{L_2} = [\,u_1-u_2 \quad v_1-v_2 \quad w_1-w_2 \quad p_1-p_2\,]^T, \tag{22}$$

in which the matrices $\mathbf{A_1}$, $\mathbf{A_2}$, $\mathbf{B_1}$, $\mathbf{B_2}$ are written as detailed in the Appendix A.

2.4. Active control

For active control, the surface pressure of the acoustic wave at the center of the radiating plate (point A in Fig. 1) has been chosen as the control objective instead of the vibration displacement at point A, because some vibrational modes of this plate cannot be controlled by using the central vibration displacement as the objective function. In the COMSOL environment, a piezo solid mode is used to model the piezoelectric patches glued onto the two sides of the excited plate. Supposing that P_{in} is the pressure of the incident acoustic wave and V_{imp} is the voltage imposed on the piezoelectric patches, the active behavior of the double-wall active sound package can be obtained in three steps under the condition that this sound package is a linear system. Fig. 1 shows the transfer function schematic of double-wall active systems.

(1) $P_{in} = P_0$, $V_{imp} = 0$

The pressure P_{in} of the incident acoustic wave is chosen to be P_0, and the voltage V_{imp} is zero, that is, the active control is turned off. The surface pressure of the acoustic wave at the radiating side can be calculated and represented as $w_p(\omega)$. Then the first transfer function of the incident wave can be written as

$$H_p(\omega) = \frac{w_p(\omega)}{P_0}. \tag{23}$$

(2) $P_{in} = 0$, $V_{imp} = V_0$

In this step, no more incident wave is transmitted into the double-wall active sound package, and an electric potential V_0 applied to the piezoelectric patches is imposed on the excited plate. Once again, the surface pressure of the acoustic wave at the radiating side can be calculated and represented as $w_s(\omega)$. Therefore, the second transfer function of the secondary sound source can be written as

$$H_s(\omega) = \frac{w_s(\omega)}{V_0}. \tag{24}$$

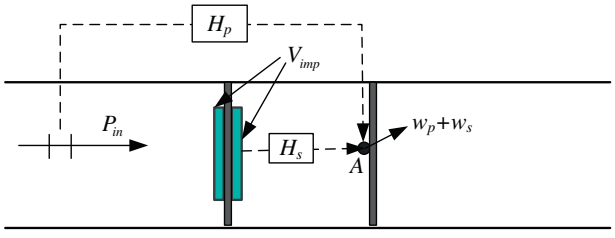

Fig. 1. The transfer function schematic of double-wall active systems.

(3) $P_{in} = P_1$, $V_{imp} = V_s$
Finally, an incident acoustic wave pressure of P_1 is imposed, and the optimal voltage exciting the plate is calculated to be

$$V_s(\omega) = -\frac{H_p(\omega)}{H_s(\omega)} P_1. \tag{25}$$

Therefore, the displacement or surface pressure of the acoustic wave at the radiating side can be reduced significantly.

2.5. Transmission loss

The acoustic performance of the double-wall active sound packages is described by the transmission loss as defined in Eq. (26).

$$TL_{dB} = 10\lg(W_i/W_t), \tag{26}$$

where W_i and W_t are the amplitudes of the incident and transmitted wave energies, respectively. In the COMSOL environment, only plane waves under normal incidence are considered, and no reflection occurs in the rear of the packages.

3. Experiment

A transmission-loss measurement was carried out in a rectangular tube to validate the finite element models of the double-wall active sound packages. The cross-section of the rectangular tube was 66 × 66 mm^2, and its cut-off frequency was 2500 Hz, which allowed the transmittance of a normal plane wave in the tube. The secondary acoustic source was controlled by the classical FXLMS algorithm implemented on a dSPACE-DS1103 controller with Simulink. Only one error sensor located on the front of the radiating plate was used for active control.

3.1. The measurement with a two source-location method

The two source-location method was applied to measure the scattering matrix of the sound packages, from which the transmission loss could be calculated. The measurement characterization of the two source-location method is shown in Fig. 2. The definition of the scattering matrix is provided by Eq. (27), which gives the linear relationships between the incoming pressure wave vector $\{P^+(z^{\mathrm{up}}), P^-(z^{\mathrm{dn}})\}^T$ and the outgoing pressure wave vector $\{P^-(z^{\mathrm{up}}), P^+(z^{\mathrm{dn}})\}^T$.

$$\begin{Bmatrix} P^-(z^{\mathrm{up}}) \\ P^+(z^{\mathrm{dn}}) \end{Bmatrix} = [D]_{2\times 2} \begin{Bmatrix} P^+(z^{\mathrm{up}}) \\ P^-(z^{\mathrm{dn}}) \end{Bmatrix}, \tag{27}$$

Eq. (27) shows that the incoming and outgoing pressures on both sides of the samples are needed to calculate the scattering matrix. Microphones, however, measure the total sound pressure; hence, at least two measuring points on each side are required to separate the incoming and outgoing pressures from the total pressure. However, due to the presence of standing waves in the tube, the spacing between the two measuring points cannot be equal to an integer multiple of the half-wavelength of the broadband noise excitation, and the spacing must also satisfy the condition $d < 2c_0/5f_{\max}$ [48], where c_0 is the sound speed and $f_{\max}$ is the maximum measuring frequency. In addition, if some measuring points are adjacent to the nodes of some singularity frequencies, the measurement error will be increased due to the low signal-to-noise ratio (SNR); hence, additional measuring points should be set on both sides of the tested structure to eliminate this phenomenon. In this study, four measuring points on each side were used, and the scattering matrix was calculated by the expression as follows:

$$[D]_{2\times 2} = [P^{out}]_{2\times 2} \cdot [P^{in}]^{-1}_{2\times 2}. \tag{28}$$

Here,

$$[P^{out}]_{2\times 2} = \begin{bmatrix} P^{-(1)}(z^{\mathrm{up}}) & P^{-(2)}(z^{\mathrm{up}}) \\ P^{+(1)}(z^{\mathrm{dn}}) & P^{+(2)}(z^{\mathrm{dn}}) \end{bmatrix}_{2\times 2} \quad \text{and}$$

$$[P^{in}]_{2\times 2} = \begin{bmatrix} P^{+(1)}(z^{\mathrm{up}}) & P^{+(2)}(z^{\mathrm{up}}) \\ P^{-(1)}(z^{\mathrm{dn}}) & P^{-(2)}(z^{\mathrm{up}}) \end{bmatrix}_{2\times 2},$$

where $P^{\pm(i)}(z^{\mathrm{up}})$ and $P^{\pm(i)}(z^{\mathrm{dn}})$ represent the incoming and outgoing waves in the ith excitation source, $i = 1,2$.

$$\begin{Bmatrix} P^+(z^{\mathrm{up}}) \\ P^-(z^{\mathrm{up}}) \end{Bmatrix} = \left[[Md^{\mathrm{up}}]^H_{2\times 4} \cdot [Md^{\mathrm{up}}]_{4\times 2} \right]^{-1} \cdot [Md^{\mathrm{up}}]^H_{2\times 4} \cdot \left\{ P(z_i^{\mathrm{up}}) \right\}_{4\times 1}, \tag{29}$$

$$\begin{Bmatrix} P^+(z^{\mathrm{dn}}) \\ P^-(z^{\mathrm{dn}}) \end{Bmatrix} = \left[[Md^{\mathrm{dn}}]^H_{2\times 4} \cdot [Md^{\mathrm{dn}}]_{4\times 2} \right]^{-1} \cdot [Md^{\mathrm{dn}}]^H_{2\times 4} \cdot \left\{ P(z_i^{\mathrm{dn}}) \right\}_{4\times 1}. \tag{30}$$

Here, the superscript H denotes the conjugate transpose, and $P(z_i^{\mathrm{up}})$ and $P(z_i^{\mathrm{dn}})$ represent the pressures measured by the ith microphone, $i = 1, \ldots, 4$. In the following expressions, $d_1, \ldots, d_3$ are the spacing measurements between the microphones:

$$[Md^{\mathrm{up}}]_{4\times 2} = \begin{bmatrix} 1 & e^{jkd_1} & e^{jkd_2} & e^{jkd_3} \\ 1 & e^{-jkd_1} & e^{-jkd_2} & e^{-jkd_3} \end{bmatrix}^T,$$

$$[Md^{\mathrm{dn}}]_{4\times 2} = \begin{bmatrix} 1 & e^{-jkd_1} & e^{-jkd_2} & e^{-jkd_3} \\ 1 & e^{jkd_1} & e^{jkd_2} & e^{jkd_3} \end{bmatrix}^T. \tag{31}$$

Therefore, the transmission loss can be calculated from the D_{21} element of the scattering matrix, which is the transmission coefficient in the positive z direction.

$$TL = 10\lg(1/|D_{21}|^2). \tag{32}$$

3.2. Experimental disposition

The experimental apparatus consisted of four parts: the source, the test section, the control system and the data processing. The two sources used in the experiments generated white noise signals with an emission band of 50–2000 Hz, and one of the sources

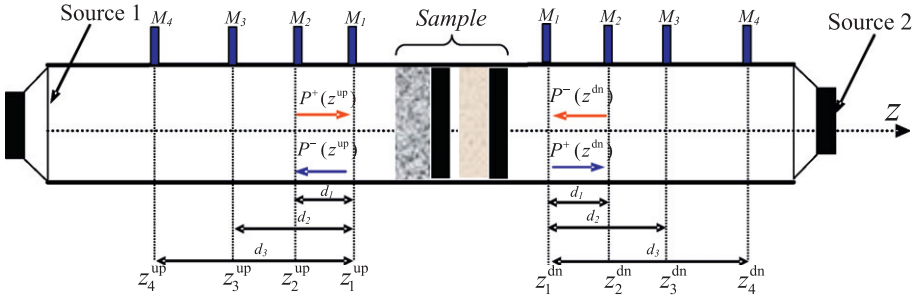

Fig. 2. The measurement of two source-location method.

located on the upstream of the test section was the primary source. The piezoelectric ceramics that were added onto the excited plate behaved as the secondary source.

The tested structure was installed in the test section, and each layer of the structure was fixed on a frame that could slide freely in the tube. These frames could be used to isolate air layers with different thicknesses and quickly form different multilayer active acoustic structures. The radiating and excited plates each had an area slightly larger than the cross-section of the tube, and the two plates were adhered to the frame, whereas the porous material had the same cross-section as the tube and was simply embedded in the frame.

In the two source-location measurement, a Siglab dynamic system analyzer generated the broadband noise signals and then transmitted them to source 1 or source 2. In the active-control scenario, the error sensor signal was amplified and filtered, and then it was controlled by the classical FXLMS algorithm implemented on a dSPACE-DS1103 controller with Simulink to determine the control signal. Fig. 3 shows the characterization of the control system and data processing. The microphones used for the acoustic pressure measurements were B&K 1/4 4939-type. The pressure signals were pre-amplified with a gain of 10 dB.

3.3. The error analysis of measurements

In this section, the measurement error of the two-source-location method is analyzed to ensure that the transmission loss calculated by the measured pressures is accurate and valid. In effect, the transmission loss is obtained by measuring the pressures on both sides of the tested structure; hence, the error on TL_{dB} depends on the measurement error on the pressures. Eqs. (29) and (30) show that the incoming and outgoing waves on both sides of the tested structure are related to the microphones' errors and their position errors; however, the position error is negligible, so only the microphone errors must be considered. For convenience of analysis, considering only the two measuring points on each side, the vectors $[Md^{up}]$ and $[Md^{dn}]$ can be rewritten as

$$[Md^{up}]_{2\times2} = \begin{bmatrix} 1 & 1 \\ e^{jkd_1} & e^{-jkd_1} \end{bmatrix}, \quad [Md^{dn}]_{2\times2} = \begin{bmatrix} 1 & 1 \\ e^{-jkd_1} & e^{jkd_1} \end{bmatrix}. \tag{33}$$

The incoming and outgoing waves on the left side of the tested structure (the right side can be treated similarly) can be formulated as

$$\begin{bmatrix} P^+(z^{up}) \\ P^-(z^{up}) \end{bmatrix} = [Md^{up}]^{-1}_{2\times2} \cdot \{P(z_i^{up})\}_{2\times1} = \frac{1}{2\sin kd_1} \begin{bmatrix} e^{-jkd_1} & 1 \\ e^{jkd_1} & 1 \end{bmatrix} \begin{bmatrix} P(z_1^{up}) \\ P(z_2^{up}) \end{bmatrix}. \tag{34}$$

It can be seen that Eq. (34) is solvable under the condition that $\sin kd_1 \neq 0$, that is, the spacing d_1 between the two microphones cannot be an integer multiple of the half-wavelength. Otherwise, Eq. (34) is insolvable, invalidating the measurement. Suppose that P is the truth-value of $\begin{bmatrix} P(z_1^{up}) & P(z_2^{up}) \end{bmatrix}^T$ and that its measuring error is ΔP, which induces a calculated error ΔR of $\begin{bmatrix} P^+(z^{up}) & P^-(z^{up}) \end{bmatrix}^T$, for which the associated truth-value is R. If the matrix $[Md^{up}]^{-1}_{2\times2}$ is non-singular, the relation between the relative errors of R and P can be expressed as [49]

$$0 \leqslant \frac{\|\Delta R\|_1}{\|R\|_1} \leqslant \frac{2}{|\sin kd_1|} \frac{\|\Delta P\|_1}{\|P\|_1}. \tag{35}$$

Here, $\|\|_1$ denotes the first norm of a matrix. Because $\frac{\|\Delta R\|_1}{\|R\|_1} = \frac{|\Delta P^+(z^{up})|+|\Delta P^-(z^{up})|}{|P^+(z^{up})|+|P^-(z^{up})|}$, Eq. (36) can be obtained with an inequality operation:

$$0 < \frac{|\Delta P^+(z^{up})|}{|P^+(z^{up})|} \leqslant \frac{4}{|\sin kd_1|} \frac{\|\Delta P\|_1}{\|P\|_1}. \tag{36}$$

Similarly,

$$0 < \frac{|\Delta P^+(z^{dn})|}{|P^+(z^{dn})|} \leqslant \frac{4}{|\sin kd_1|} \frac{\|\Delta P\|_1}{\|P\|_1}. \tag{37}$$

Suppose that TL is the truth-value of TL_{dB} and that its calculated value is TL^*; the error $\Delta TL = TL - TL^*$ can be written as

$$\Delta TL = 20\lg \frac{|1 - \Delta P^+(z^{dn})/P^+(z^{dn})|}{|1 - \Delta P^+(z^{up})/P^+(z^{up})|}. \tag{38}$$

Eq. (38) can be further simplified [49]:

$$|\Delta TL| \leqslant 20\lg \frac{1 + |\Delta P^+(z^{dn})/P^+(z^{dn})|}{1 - |\Delta P^+(z^{up})/P^+(z^{up})|}. \tag{39}$$

Suppose that $\pm\delta$dB is the microphone error. Then, the corresponding maximum relative error of the sound pressure can be written as $\eta = |\Delta P|/|P| = 10^{\delta/20} - 1$, and the range of ΔTL can be deduced from Eqs. (36), (37) and (39):

$$|\Delta TL| \leqslant 20\lg \frac{1 + 4\eta/|\sin kd_1|}{1 - 4\eta/|\sin kd_1|}, \tag{40}$$

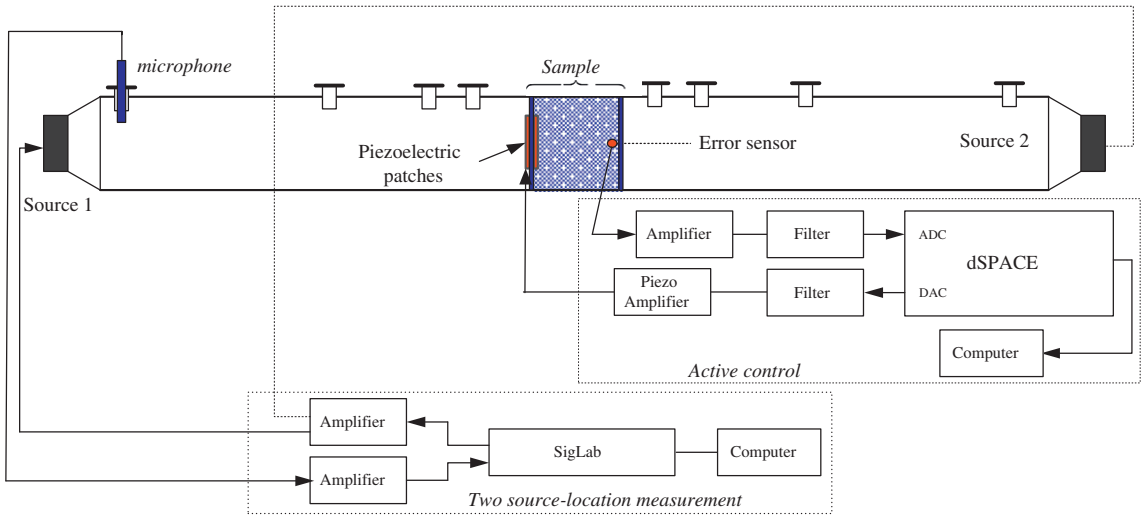

Fig. 3. The characterization of the control system and data processing.

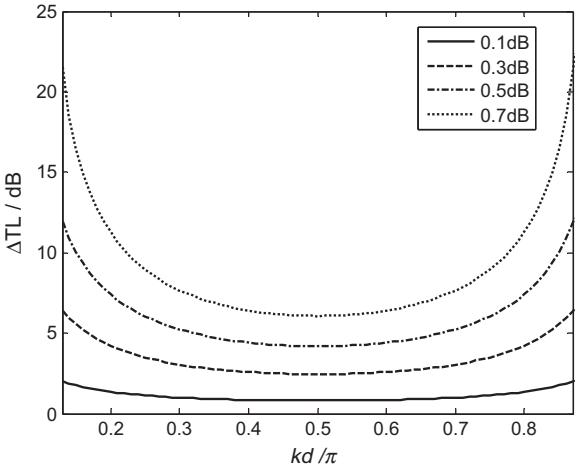

Fig. 4. The relationship between ΔTL, the microphone's error and spacing.

Eq. (40) shows that ΔTL depends on kd_1 and δ; hence, the functional description of their relationships can be drawn in the $(0,\pi)$ interval, as shown in Fig. 4. To ensure that ΔTL does not exceed 5 dB, the condition $(0.3+n)\pi \leqslant kd_1 \leqslant (0.7+n)\pi$ must be satisfied and the microphone error must be within ±0.5 dB. When the microphone error is known, ΔTL reaches a minimum under the condition that $kd_1 = (0.5+n)\pi$, $n = 0, 1, \ldots$; therefore, the optimal spacing between the microphones is 1/4 of the wavelength of the frequency of interest.

4. Numerical and experimental validations

In this section, the results of the numerical and experimental evaluation of the sound transmission performance of the double-wall active packages and their constituent layers are presented. The numerical results obtained from the COMSOL environment are validated by experiments, and the properties of the materials used in this study are given in Table 1. For each structure, only one quarter of the structure was modeled in COMSOL to reduce the memory storage and time cost, and $5\times5\times1$, $5\times5\times2$, $5\times5\times2$ and $4\times4\times1$ 3D meshes were applied, respectively, to the plate, the air gap, the porous material and the piezoelectric patches. Each type of element used in COMSOL was quadratic. For each structure, the computational performance was good, and the maximum computation time did not exceed 4 h.

Table 1
Materials' properties for the double-wall structures.

Radiating plate	
Thickness	0.2 mm
Mass density	7700 kg/m^3
Young's modulus	2.16e11 N/m^2
Poisson's ratio	0.27
Excited plate	
Thickness	0.2 mm
Mass density	7700 kg/m^3
Young's modulus	2.16e11 N/m^2
Poisson's ratio	0.27
Piezo ceramic	
Thickness	0.5 mm
Mass density	7760 kg/m^3
Young's modulus	9.6e10
Poisson's ratio	0.34
Coupling (C/N)	−2.14e−10
Relative permittivity	2109
Compliance (1/Pa)	−7.107e−12

4.1. Sound leakage analysis

The rectangular tube used in the measurements was made of steel with a thickness of 15 mm, and the upstream, downstream and test sections were bonded by rivets, which could induce sound leakage in the tube. Therefore, a measurement was carried out to analyze the sound leakage in the condition that no test structure was installed in the test section.

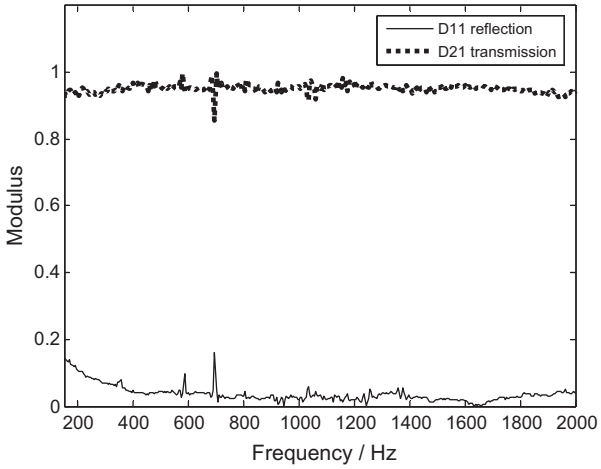

Fig. 5. The reflection and transmission coefficients of the tube without tested structure.

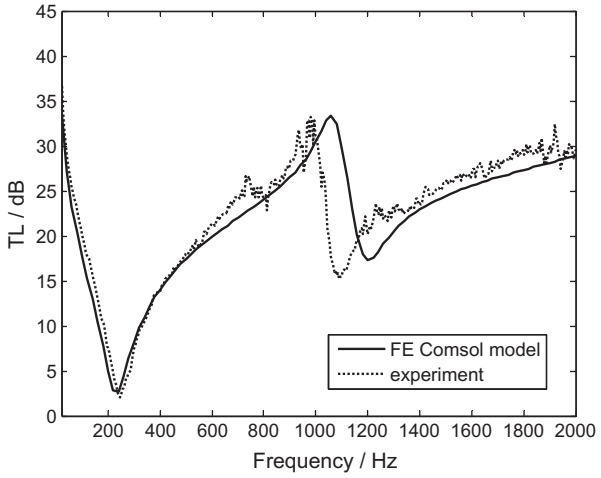

Fig. 6. Transmission loss of the radiating plate with simply support.

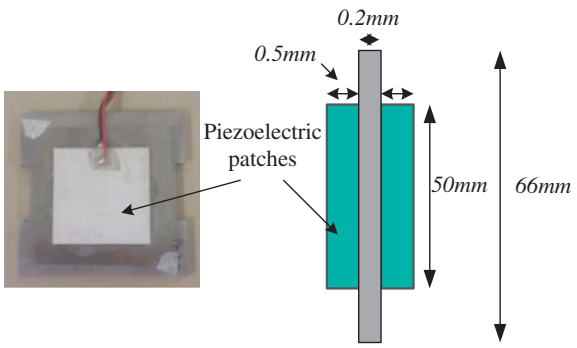

Fig. 7. The configuration of the excited plate.

Fig. 5 shows the modulus of the reflection and transmission coefficients (D_{11} and D_{21}) of the tube with no test structure installed. In this case, the ideal transmission coefficient would be equal to one and the ideal reflection coefficient would be zero; because there was no test structure in the test section, no sound should have been reflected and all acoustic waves should have been transmitted. However, the measurement result shows that the transmission coefficient was equal to 0.95 and that the reflection coefficient was near to 0.02 in the all-range frequency. Hence, the crack between each section allowed 5% of the sound energy to be leaked, and the remaining 95% of the sound wave could be transmitted through the test structure. This sound leakage produced a −0.45 dB correction to the transmission loss, which is slight and could be ignored in the measurements.

4.2. The radiating plate

The radiating plate used in the double-wall active sound packages was a normal steel panel with a thickness of 0.2 mm. In the COMSOL environment, only a quarter of this simple support plate was modeled because of its symmetry, reducing the required memory storage and calculation time. This radiating plate was excited by a normal plane wave, and its transmission loss results are given in Fig. 6 for the numerical and experimental cases. The two results show that the first resonance frequency of the radiating plate was close to 250 Hz, and good agreement can be seen at low frequency. However, some offset of the second resonance frequency is noted; this may be because a thin aluminum sheet was used to glue this plate to the framework of the test tube, which

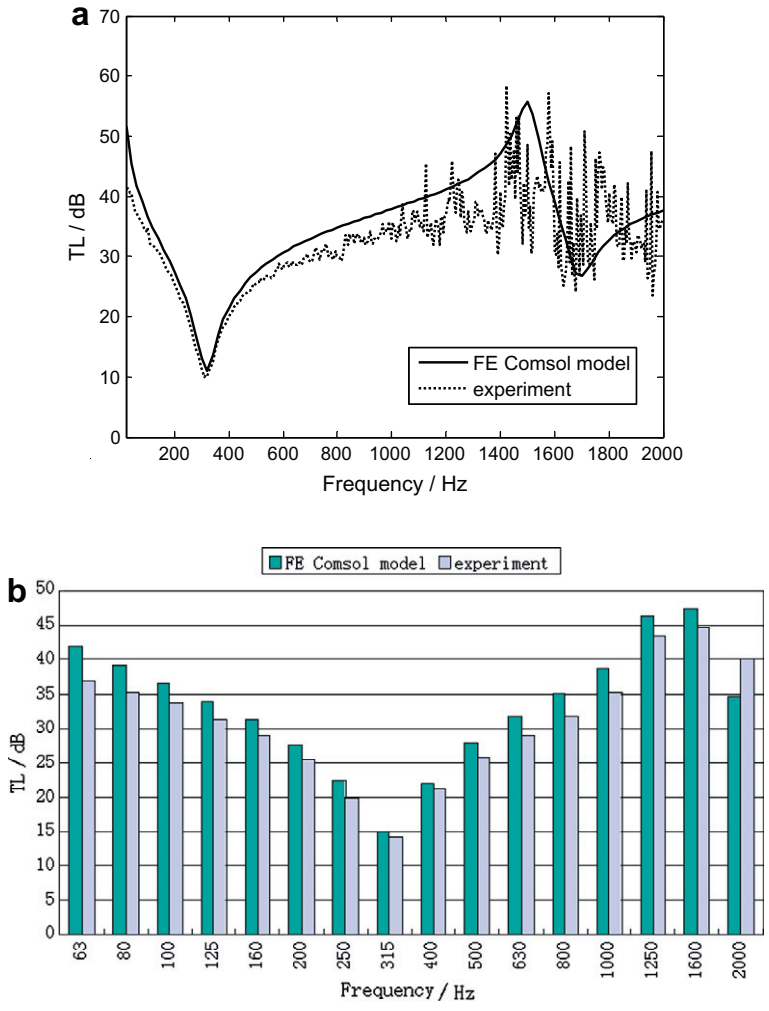

Fig. 8. Transmission loss of the excited plate with simply support: (a) TL; (b) TL on average.

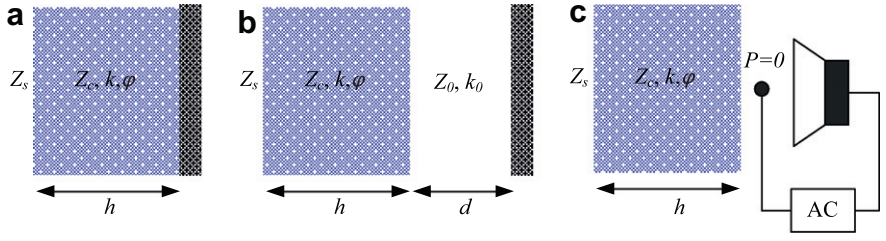

Fig. 9. Porous material with three boundary conditions: (a) with a rigid wall; (b) with a layer of air; (c) active condition.

may have changed the attributes of the plate and caused a shift in the resonance frequency.

4.3. The excited plate

The configuration of the excited plate with piezoelectric patches is shown in Fig. 7, and its parameters are also given in Table 1. Fig. 8a presents the transmission loss in the experiment and the simulation under the condition of no excitation of the piezoelectric patches. With the piezoelectric patches glued onto the excited plate, its first resonance frequency shifted to 320 Hz, and its transmission loss was improved due to the piezoelectric patches increasing the thickness of the excited plate as compared with the radiating plate. Fig. 8b shows the transmission loss of the excited plate on average at the center frequency of 1/3 octave. It shows that the experimental results and the simulation match each other very well, and the discrepancy is less than 5 dB.

4.4. Porous material

In most problems, the hypothesis of a rigid skeleton for the porous material is valid, and the medium behaves as a visco-thermal equivalent fluid. However, this assumption is not adopted in this work because the active control procedure must be efficient over low frequencies, where strong coupling between the solid and fluid phases occurs in the poroelastic material. In the COMSOL environment, a PDE model was used to model this poroelastic material. The surface impedance Z_s at normal incidence was calculated in three boundary condition limits, as shown in Fig. 9: with a rigid wall, with a layer of air and under the active control condition, that is, with zero pressure at the rear of the poroelastic medium. In the Biot–Allard theory, the surface impedance is calculated with Eqs. (41)–(43). Z_c, k and Z_0, k_0 are the impedances and wave numbers of the porous material and the air layer, respectively.

(1) With a rigid wall, Fig. 9a

$$Z_s = -j\frac{Z_c}{\phi}\cot(kh). \tag{41}$$

(2) With a layer of air, Fig. 9b

$$Z_s = \frac{Z_c}{\phi}\frac{-jZ_a\cot(kh)+Z_c}{Z_a - jZ_c\cot(kh)}. \tag{42}$$

Here, $Z_a = -jZ_0\cot(kd)$.

(3) Under the active control condition, Fig. 9c

$$Z_s = \frac{Z_c}{\phi}\tan(kh). \tag{43}$$

However, in the COMSOL environment, Z_s is defined as the ratio of the acoustic pressure and the total velocity at the impinged face, and it can be written as

$$Z_s(\omega) = \frac{p}{j\omega\left(\phi U_3^f + (1-\phi)u_3^s\right)} = p\cdot\left\{j\omega\left[\frac{\phi}{\omega^2\tilde{\rho}_{22}}p_z + \left(1-\phi\left(1+\frac{\tilde{\rho}_{12}}{\tilde{\rho}_{22}}\right)\right)w\right]\right\}^{-1}. \tag{44}$$

To confirm that the PDE model modeling this poroelastic material was available in COMSOL, we calculated the ratio of the surface impedance to the air impedance, Z_s/Z_0, by applying the Biot–Allard

Table 2
Parameters of porous materials (felt).

Thickness	25 cm
Porosity	0.93
Resistivity	23,150 rayls/m
Young's modulus	12,000 Pa
Mass density	50 kg/m^3
Tortuosity	1.1
Viscous length	44 μm
Thermal length	121 μm
Poisson ratio	0.06

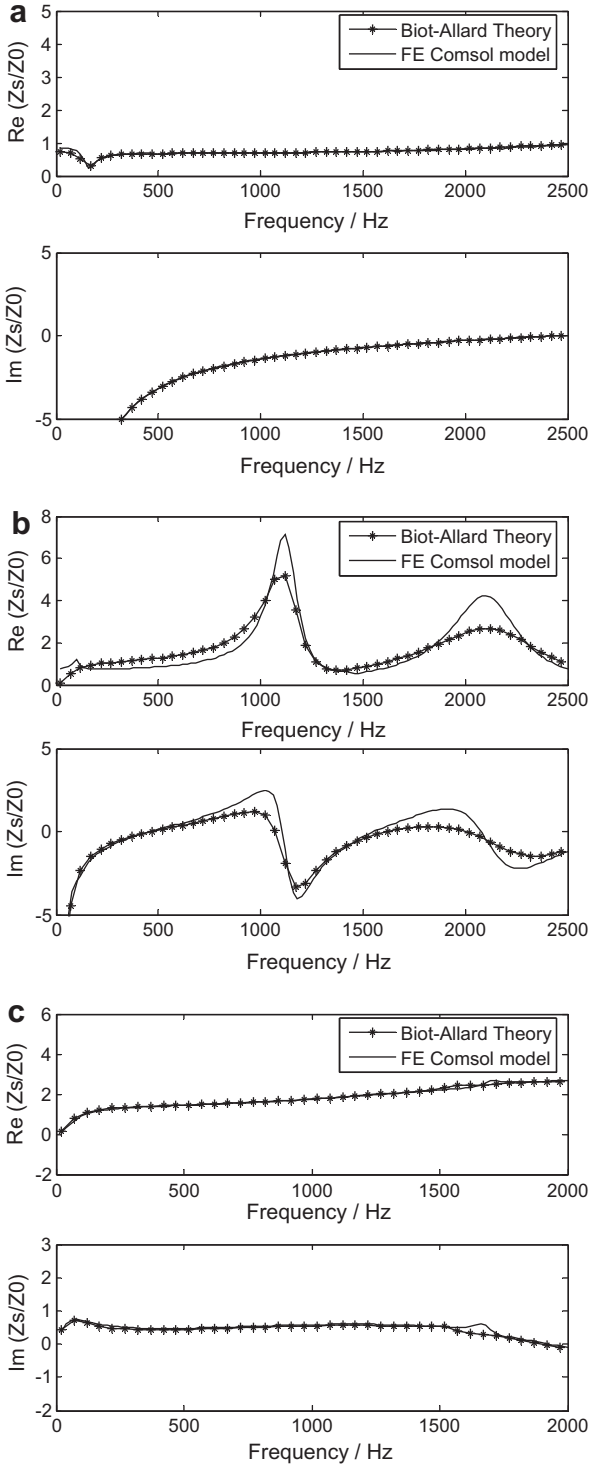

Fig. 10. Comparison of surface impedance in Biot–Allard theory and FE Comsol model: (a) with rigid wall; (b) with a layer of 12 cm air; (c) active condition.

theory to some examples, given in Table 2, which have been validated with experimental measurements [50]. By comparing to the results obtained in COMSOL with the finite element method, good agreement can be noted for the three boundary conditions, as shown in Fig. 10.

The properties of the porous material used in this study as cores for the double-wall active sound packages are shown in Table 3. The acoustical performance curves of this porous material backed by an air gap are shown in Fig. 11 for both the experiment and the simulation. The first resonance frequency of this material was about 360 Hz, and its absorption coefficient was excellent (more than 0.8 for all frequencies of interest), whereas its transmission loss was less than 8 dB. Good agreement between the numerical and experimental results was obtained for the frequency of interest, and the discrepancy between the two methods does not exceed 1 dB.

Table 3
Parameters of the porous materials (felt).

Thickness	20 mm
Porosity	0.95
Resistivity	14,750 rayls/m
Shearing modulus	$55{,}000 * (1 + j * 0.055)$ N/m^2
Mass density	100 kg/m^3
Tortuosity	1.1
Viscous length	37 μm
Thermal length	196 μm
Poisson ratio	0.3

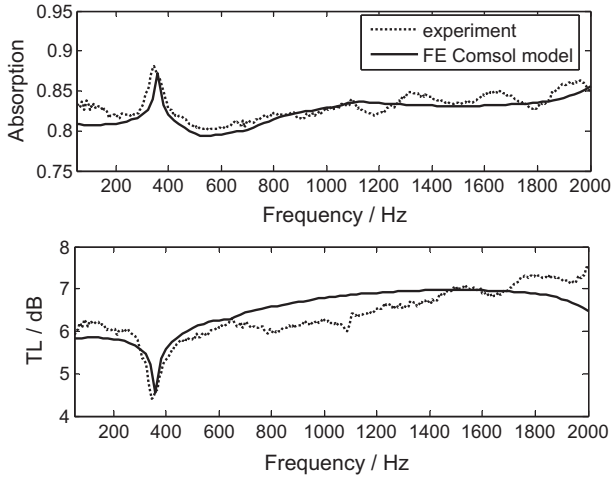

Fig. 11. The acoustical performance of the porous material.

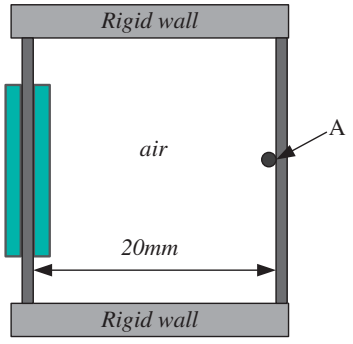

Fig. 12. The configuration of the double-wall structure with air gap.

4.5. Double-wall active sound packages

Some examples of double-wall active sound packages with different cores are presented in this section. The numerically and experimentally determined transmission losses of these packages are given, and both methods demonstrate that clear improvements in the performance of the packages can be obtained by active control.

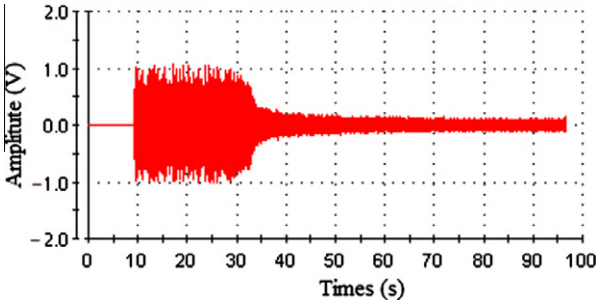

Fig. 13. The error sensor signals in point A before and after active control.

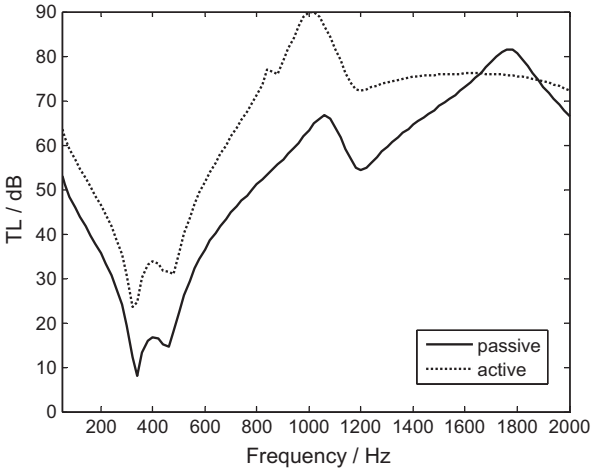

Fig. 14. Transmission loss of a double-wall structure with air gap in simulation with passive and active control.

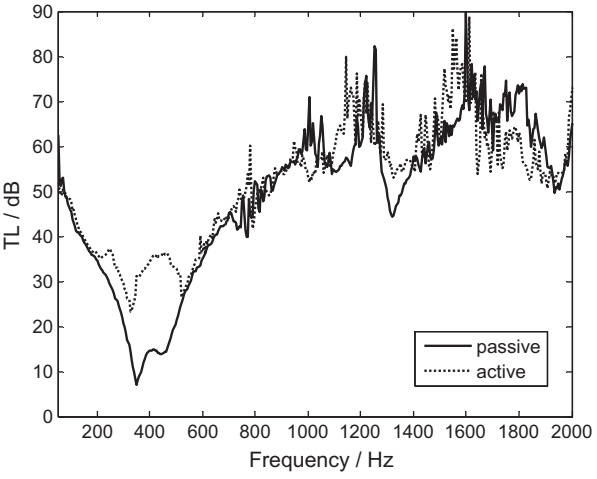

Fig. 15. Transmission loss of a double-wall structure with air gap in experiment with passive and active control.

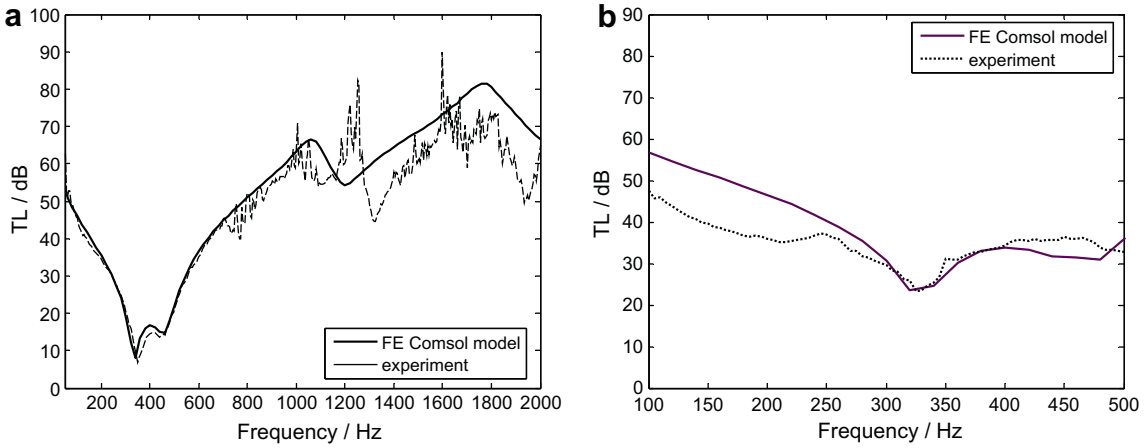

Fig. 16. Comparison in transmission loss of a double-wall structure with air gap in simulation and experiment: (a) passive; (b) active.

4.5.1. A double-wall structure with air gap

A configuration of a double-wall active sound package with an air gap of 20-mm thickness is shown in Fig. 12. In this configuration, we treated the air as an ideal medium, and therefore its viscosity and damping were neglected. An error sensor was positioned in point A, and the experimental signals from this error sensor both with and without active control are shown in Fig. 13. Obvious reduction in transmission loss could be seen under active control, and the cost time to reach the minimum pressure was short.

In the COMSOL environment, $5 \times 5 \times 1$, $5 \times 5 \times 2$ and $4 \times 4 \times 1$ 3D meshes were applied to the plate, the air gap and the piezoelectric patches, respectively. The numerical and experimental results concerning the transmission loss of this double-wall structure with both passive and active control, using the minimum pressure at point A, are shown in Figs. 14 and 15. The resonance frequencies of the double-wall structure were 340 Hz and 460 Hz, according to the numerical results, while they were observed to be 350 Hz and 440 Hz in the experiment; the relative error between the two methods was less than 5%. The first resonance frequency is the first mode frequency of the active plate, and the second resonance frequency is the resonance frequency of the structure. Fig. 14 shows that the active control should be valid up to 1600 Hz and that about a 15-dB improvement in the transmission loss can be obtained at the resonance frequencies in the numerical results; Fig. 15 shows that a gain of approximately 15 dB was obtained near the resonance frequencies in the experiment and that no improvement could be realized with active control at frequencies greater than 500 Hz. The reason for this discrepancy is that the active control was only operated at less than 500 Hz in the experiment to avoid destroying the piezoelectric ceramic with high voltage. It should be noted that no improvement was obtained at frequencies below 100 Hz in the experiment due to the very low voltage imposed on the piezoelectric ceramic, which meant that

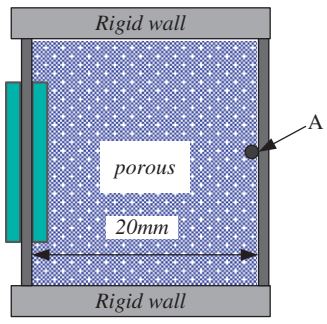

Fig. 17. The configuration of the double-wall structure with porous material.

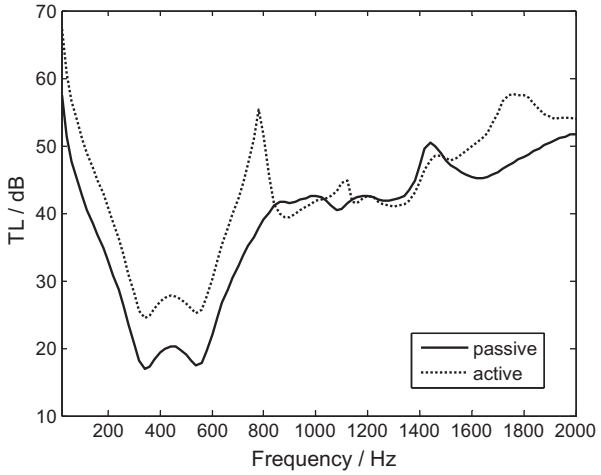

Fig. 18. Transmission loss of a double-wall structure with porous material in simulation with passive and active control.

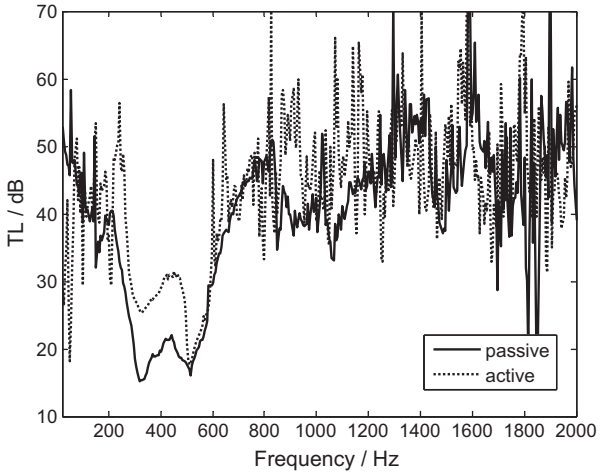

Fig. 19. Transmission loss of a double-wall structure with porous material in experiment with passive and active control.

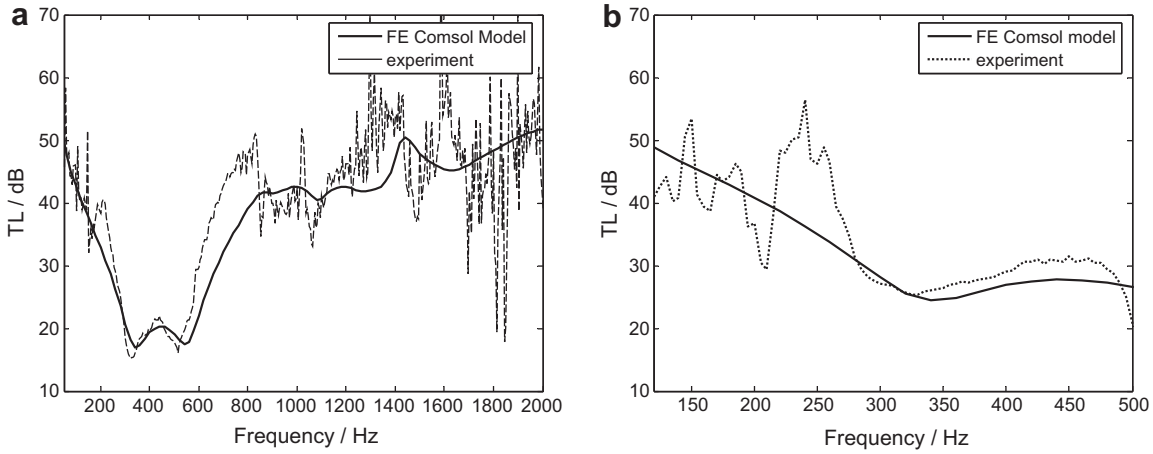

Fig. 20. Comparison in transmission loss of a double-wall structure with porous material in simulation and experiment: (a) passive; (b) active.

the excited plate could not vibrate as a secondary source at these low frequencies, invalidating the active control. For the purpose of clear illustration, Fig. 16 presents a comparison between the numerical and experimental transmission-loss results. The comparison shows that without active control, the transmission loss seen in the experimental measurement was in good agreement with the numerical all-range frequency result of the finite element method. With active control, the two results matched each other very well at frequencies below 500 Hz.

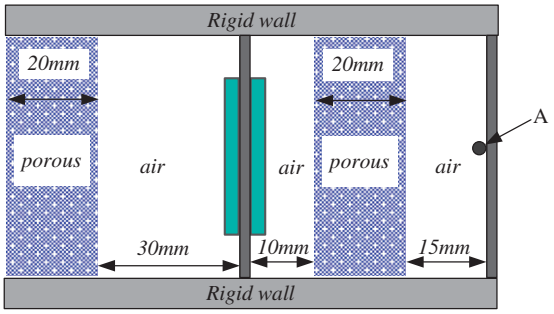

Fig. 21. The configuration of Cell A.

4.5.2. A double-wall structure with porous material

The numerically and experimentally determined transmission losses of the double-wall package after changing the air gap to a porous-material core with the same thickness (see Fig. 17) are shown in Figs. 18 and 19. In this configuration, the viscous damping of the porous material is represented by the dynamic viscosity of air in the pores when modeling it in the (u,p) formulation. In the COMSOL simulation, $5 \times 5 \times 1$, $5 \times 5 \times 2$ and $4 \times 4 \times 1$ 3D meshes were applied to the plate, the porous material and the piezoelectric patches, respectively. The minimum pressure at point A was still used to define the active control condition. The resonance frequencies of the double-wall structure were 340 Hz and 540 Hz, according to the numerical results, while they were observed to be 320 Hz and 515 Hz in the experiment; the relative error between the two methods was less than 7%. The first resonance frequency is the first mode frequency of the active plate, and the second resonance frequency is the resonance frequency of the structure. Fig. 18 shows that the active control should be valid up to 800 Hz and that about a 10-dB improvement in the transmission loss can be obtained at the resonance frequencies in the numerical results; Fig. 19 shows that a gain of approximately 10 dB was obtained near the resonance frequency and that no improvement was obtained at frequencies below 120 Hz in the experiment due to the very low voltage imposed on the piezoelectric ceramic. In addition, the numerical and experimental results in the

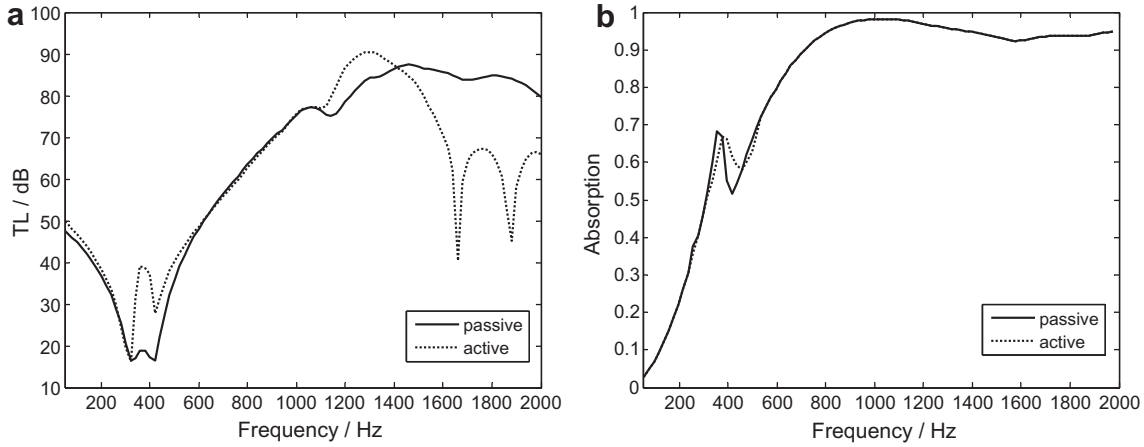

Fig. 22. Numerical results of Cell A with passive and active control: (a) transmission loss; (b) absorption coefficient.

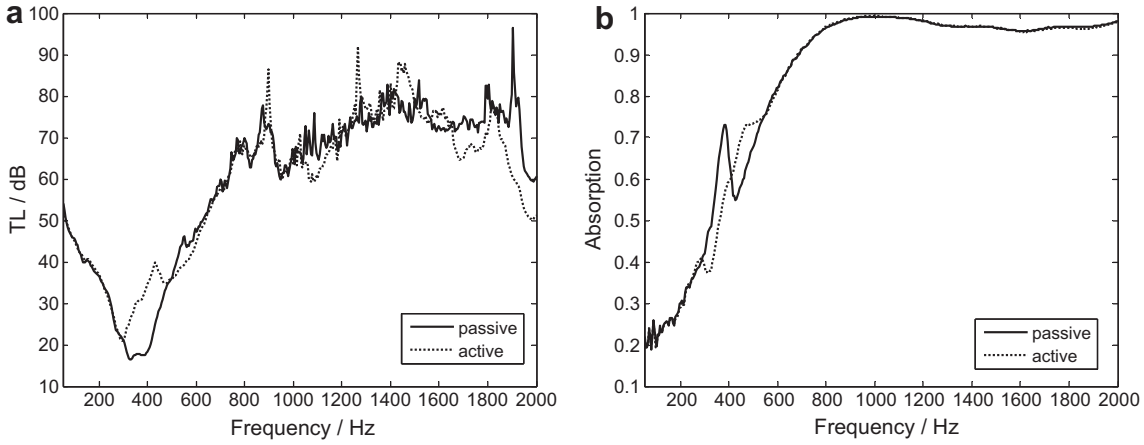

Fig. 23. Experimental results of Cell A with passive and active control: (a) transmission loss; (b) absorption coefficient.

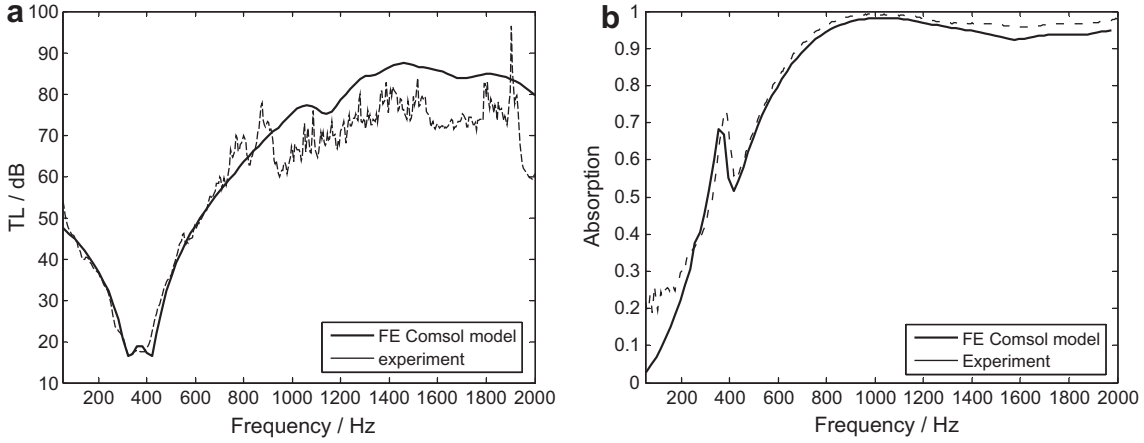

Fig. 24. Comparison of Cell A in simulation and experiment without active control: (a) transmission loss; (b) absorption coefficient.

passive-control scenario show that the transmission loss at the resonance frequencies of the double-wall structure was noticeably improved by the use of a porous-material core, as compared to that achieved with an air–gap core. For the purpose of clear illustration, Fig. 20 presents a comparison between the numerical and experimental transmission-loss results. The comparison shows that without active control, the transmission loss seen in the experimental measurement was in good agreement with the numerical all-range frequency result of the finite element method. With active control, the two results matched each other very well at frequencies below 500 Hz.

4.5.3. A double-wall structure with several layers

A complex double-wall structure with several air gaps and porous materials, named 'Cell A' (Fig. 21), is presented in this section. The reason for choosing these layers is that this composition is efficient for both absorption and insulation [51], because the porosity, resistivity and thickness of the porous material and the air layer located at the front of the excited plate strongly affect the sound absorption and insulation performance of the double-wall structure. The transmission losses and absorption coefficients of Cell A as determined by numerical simulation and experimental measurement are shown in Figs. 22 and 23, respectively. The same meshes as previously noted were applied to the layers, and the minimum pressure at point A was still used to define the active control condition. The resonance frequencies of the double-wall structure were 320 Hz and 420 Hz, according to the numerical results, while they were observed to be 325 Hz and 400 Hz in the experiment; the relative error between the two methods was less than 5%. The first resonance frequency is the first mode frequency of the active plate, and the second resonance frequency is the resonance frequency of the structure. In the 300–500 Hz frequency range, a 15-dB improvement could be achieved in the transmission loss in both the numerical results and the experiment, whereas the absorption coefficient exhibited a small offset in both results. In addition, the absorption coefficient in both the numerical and experimental results exceeded 0.6 at frequencies greater than 500 Hz. For the purpose of clear illustration, Fig. 24 presents a comparison between the numerically and experimentally determined transmission losses and absorption coefficients. The comparison shows that without active control, the transmission loss seen in the experimental measurement matched well with the numerical all-range frequency result of the finite element method. The absorption coefficients of this structure evaluated by the two methods matched each other very well, and the absolute error did not exceed 0.1 at the frequency of interest.

5. Conclusions

The acoustical transmission performance of double-wall active sound packages subjected to a plane wave excited in a rectangular tube was studied via two approaches. In the numerical approach, the poroelastic mixed (u,p) formulation was developed in the COMSOL environment for modeling the porous-material layer of

the double-wall active packages. Boundary conditions on the coupling surfaces of the elastic, poroelastic and air layers were formulated in COMSOL modes. In the experimental approach, a two source-location method was applied to measure the transmission loss of the double-wall packages, using piezoelectric ceramics as the secondary source. It has been shown that the acoustical transmission performance of double-wall active sound packages at their resonance frequencies can be improved with active control, and the numerical and experimental results agreed with each other well.

Some experimental examples have been considered to illustrate the theoretical results obtained in the COMSOL environment. Firstly, the validity of the transmission loss of each layer in the double-wall structures was demonstrated, and the surface impedance of the porous materials was validated by Biot's theory under different boundary conditions. Secondly, it was both theoretically and experimentally demonstrated that a gain of more than 10 dB in the sound insulation performance of the double-wall active sound packages can be obtained at the resonance frequencies with active control. To ensure the minimum possible error on the measurement of the transmission loss in the experiment, the microphones were chosen to have a precision within ±0.5 dB, and their spacing was set equal to 1/4 of the wavelength of the frequency of interest.

Appendix A

In Eqs. (20) and (21),

$$\mathbf{A_1} = \begin{bmatrix} 1 \\ 1 \\ 1 \\ \omega^2\phi_2^2/\phi_1^2 \end{bmatrix}^T,$$

$$\mathbf{B_1} = \begin{bmatrix} [\phi_1(1+Q_1/R_1)-\phi_2(1+Q_2/R_2)]p_1 n_x \\ [\phi_1(1+Q_1/R_1)-\phi_2(1+Q_2/R_2)]p_1 n_y \\ [\phi_1(1+Q_1/R_1)-\phi_2(1+Q_2/R_2)]p_1 n_z \\ \omega^2\left((\tilde{\rho}_{12}^{(1)}+\tilde{\rho}_{12}^{(1)})/\phi_1^2-(\tilde{\rho}_{12}^{(2)}+\tilde{\rho}_{12}^{(2)})/\phi_2^2\right)(u_1 n_x+v_1 n_y+w_1 n_z) \end{bmatrix},$$

$$\mathbf{A_2} = \begin{bmatrix} 1 \\ 1 \\ 1 \\ \omega^2\phi_1^2/\phi_2^2 \end{bmatrix}^T,$$

$$\mathbf{B_2} = \begin{bmatrix} [\phi_2(1+Q_2/R_2)-\phi_1(1+Q_1/R_1)]p_2 n_x \\ [\phi_2(1+Q_2/R_2)-\phi_1(1+Q_1/R_1)]p_2 n_y \\ [\phi_2(1+Q_2/R_2)-\phi_1(1+Q_1/R_1)]p_2 n_z \\ \omega^2\left((\tilde{\rho}_{12}^{(2)}+\tilde{\rho}_{12}^{(2)})/\phi_2^2-(\tilde{\rho}_{12}^{(1)}+\tilde{\rho}_{12}^{(1)})/\phi_1^2\right)(u_2 n_x+v_2 n_y+w_2 n_z) \end{bmatrix}.$$

References

[1] Leug P. Process of silencing sound oscillations. German patent DRP No. 655508; 1933.
[2] Thenail D, Galland M, Sunyach M, Sunhack M. Active enhancement of the absorbent properties of a porous material. Smart Mater Struct 1994;3:18–25.
[3] Beyene S, Burdisso RA. A new hybrid passive/active noise absorption system. J Acoust Soc Am 1997;101(3):1512–5.
[4] Melon M, Herzog P, Sitel A, Galland MA. Etude unidimensionnelle d'une cellule hybride pour absorption et isolation simultanée. Acoust Tech 2010;60:46–50.
[5] Guigou C, Fuller CR. Control of aircraft interior broadband noise with foam-pvdf smart skin. J Sound Vib 1999;220:541–57.
[6] Johnson BD, Fuller CR. Broadband control of plate radiation using a piezoelectric, double-amplifier active-skin and structural acoustic sensing. J Acoust Soc Am 2000;107:876–84.
[7] Pan J, Bao C. Analytical study of different approaches for active control of sound transmission through double walls. J Acoust Soc Am 1998;103:1916–22.
[8] Fonseca PD, Sas P, Brussel HV. Experimental study of the active sound transmission reduction through a double panel test section. Acustica 1999;85:538–46.
[9] Sas P, Bao C, Augusztinovisz F, Desmet W. Active control of sound transmission through a double-panel partition. J Sound Vib 1995;180:609–25.
[10] Carneal JP, Fuller CR. Active structural acoustic control of noise transmission through double panel systems. AIAA 1995;33:618–23.
[11] Wang CY, Vaicaitis R. Active control of vibrations and noise of double wall cylindrical shells. J Sound Vib 1998;216:865–88.
[12] Gardonio P, Elliott SJ. Active control of structure-borne and airborne sound transmission through double panel. J Aircraft 1998;36:1023–32.
[13] Lee JK, Kim J, Rhee CJ, Jo CH, Choi SB. Noise reduction of passive and active hybrid panels. Smart Mater Struct 2002;11:940–6.
[14] Pietrzko S, Mao Q. New results in active and passive control of sound transmission through double wall structures. Aerospace Sci Technol 2008;12(1):42–53.
[15] Galland MA, Mazeaud B, Sellen N. Hybrid passive/active absorbers for flow ducts. Appl Acoust 2005;66:691–708.
[16] Sellen N, Hilbrunner O, Galland MA. Identification of the characteristic parameters of porous media using active control. In: 8th AIAA/CEAS aeroacoustics conference, 17–19 June, Breckenridge, Colorado. AIAA Paper, 2002: 2504; 2002.
[17] Panneton R. Comments on the limp frame equivalent fluid model for porous media. J Acoust Soc Am 2007;122(6):EL217–22.
[18] Doutres O, Dauchez N, Genevaux JM, et al. Validity of the limp model for porous materials: a criterion based on the Biot theory. J Acoust Soc Am 2007;122(4):2038–48.
[19] Doutres O, Dauchez N, Genevaux JM, et al. A frequency independent criterion for describing sound absorbing materials by a limp frame model. J Acoust Soc Am 2009;95(1):178–81.
[20] Allard JF. Propagation of sound in porous media: modeling sound absorbing materials. Elsevier; 1993.
[21] Biot MA. The theory of propagation of elastic waves in a fluid-saturated porous solid. J Acoust Soc Am 1956;28:168–91.
[22] Coyette JP, Wynendaele H. A finite element model for predicting the acoustical transmission characteristics of layered structures. Proc Inter-Noise 1995;95:1279–82.
[23] Kang YJ, Bolton JS. Finite element modeling of isotropic elastic porous materials coupled with acoustical finite elements. J Acoust Soc Am 1995;98(1):635–43.
[24] Panneton R, Atalla N. An efficient finite element scheme for solving the three-dimensional poroelasticity problem in acoustics. J Acoust Soc Am 1997;101:3287–98.
[25] Taber L. A theory for transverse deflection of poroelastic plates. J Appl Mech 1992;59:628–34.
[26] Theodorakopoulos D, Beskos D. Flexural vibrations of poroelastic plates. Acta Mech 1994;103:191–203.
[27] Leclaire P, Horoshenkov K, Cummings A. Transverse vibrations of a thin rectangular porous plate saturated by a fluid. J Sound Vib 2001;247:1–18.
[28] Leclaire P, Horoshenkov K, Swift M, Hotherall D. The vibrational response of a clamped rectangular porous plate. J Sound Vib 2001;247:19–31.
[29] Atalla N, Panneton R, Debergue P. A mixed displacement-pressure formulation for poroelastic materials. J Acoust Soc Am 1998;104(3):1444–52.
[30] Debergue P, Panneton R, Atalla N. Boundary conditions for the weak formulation of the mixed (u,p) poroelasticity problem. J Acoust Soc Am 1999;106(5):2383–90.
[31] Dazel O, Sgard F. An extension of complex modes for the resolution of finite-element poroelastic problems. J Sound Vib 2002;253(2):421–45.
[32] Dazel O, Brouard B, Depollier C, et al. An alternative Biot's displacement formulation for porous materials. J Acoust Soc Am 2007;121(6):3509–16.
[33] Dazel O, Brouard B, Dauchez N, et al. Enhanced Biot's finite element displacement formulation for porous materials and original resolution methods based on normal modes. Acta Acust 2009;95(3):527–38.
[34] Dazel O, Brouard B, Dauchez N, et al. A free interface CMS technique to the resolution of coupled problem involving porous materials, application to a monodimensional problem. Acta Acust 2010;96(2):247–57.
[35] Bermudez A, Ferrin JL, Prieto A. Finite element solution of new displacement/pressure poroelactic models in acoustics. Comput Methods Appl Mech Eng 2006;195:1914–32.
[36] Batifol C, Zielinski TG, Ichchou MN, Galland MA. A finite element study of a piezoelectric/poroelastic sound package concept. Smart Mater Struct 2007;16:168–77.
[37] Etchessahar M, Sahraoui S, Brouard B. Bending vibrations of a rectangular poroelastic plate. CR Acad Sci Paris, Ser II b 2001;329:615–20.
[38] Etchessahar M, Sahraoui S, Brouard B. Vibrations of poroelastic plates: mixed displacement-pressure modelisation and experiments. Acta Acoust 2009;95:857–65.
[39] ASTM C423-08. Standard test method for sound absorption and sound absorption coefficients by the reverberation room method, developed by Subcommittee E33.01.
[40] ISO 10534. Determination of sound absorption coefficient and impedance in 973 impedance tubes. Part 1: Method using standing wave ratio; Part 2: Transfer-function method.
[41] Apfel D, Guenther T, Bolton JS, Pope J. Development of a new sound transmission test for automotive sealant materials. SAE Trans 1997;106:2651–8.

[42] Song BH, Bolton JS. A transfer-matrix approach for estimating the characteristic impedance and wave numbers of limp and rigid porous materials. J Acoust Soc Am 2000;107(3):1131–52.
[43] Zhu BL, Luo XH. The measurement method of insulation in standing wave tube. Noise Vib Contr 2000;6:41–3.
[44] Bo Q, Zhu BL. Four-microphone method of sound transmission in the standing wave tube. Noise Vib Contr 2002;6:44–6.
[45] Peng DL, Hu P, Zhu BL. The modified computation of the complex transmission coefficient of acoustical panel-in standing wave tube. J Shanghai Jiaotong Univ 2007;41(4):649–53.
[46] Tao Z, Seybert AF. A review of current techniques for measuring muffler transmission loss. SAE Paper 03NVC-38, Warrendale, USA: SAE Int; 2001.
[47] Munjal ML. Acoustics of ducts and mufflers. New York: Wiley-interscience; 1987.
[48] Munjal ML, Doige AG. Theory of a two source-location method for direct experimental evaluation of the four-pole parameters of an aeroacoustic element. J Sound Vib 1990;141(2):323–33.
[49] Wu Haijun, Jiang Weikang, Li Liangjun. Analysis of the tolerance of sound transmission loss measured by four-microphone in standing wave tube (in Chinese). J Shanghai Jiaotong Univ 2008;42(8):1265–8.
[50] Sellen N. Modification de l'impédance de surface d'un matériau par contrôle actif (in French). Ph.D. dissertation, Ecole Centrale de Lyon, France; 2003.
[51] Hu Ying, Sitel A, Galland MA, Chen Kean. A plane wave study for improving acoustical performance of double wall systems using an active–passive method. Noise Control Eng J 2009;57(3):193–202.